The influence of aftershocks on seismic hazard analysis: A case study from Xichang and the surrounding areas

Qing Wu[1], Guijuan Lai[1], Jian Wu[2], Jinmeng Bi[1,3]

[1]Institute of Geophysics, China Earthquake Administration, Beijing, China
5 [2]China Earthquake Disaster Prevention Center, Beijing, China
[3]Tianjin Earthquake Agency, Tianjin, China

Correspondence to: Qing Wu(wuqing908@sina.com), Guijuan Lai(laigj@cea-igp.ac.cn)

Abstract: In some instances, a strong aftershock can cause more damage than the mainshock. Ignoring the influence of aftershocks may underestimate the seismic

10 hazard of some areas. Taking Xichang and its surrounding areas as an example, and based on the Seismic Ground Motion Parameter Zoning Map of China (GB18306-2015), this study used the Monte Carlo method to simulate the synthetic mainshock sequences. Additionally, the Omi-Reasenberg-Jones (Omi-R-J) aftershock activity model is used to simulate the aftershock sequences that follow mainshocks

15 above a certain magnitude threshold. Then, the mainshock and the aftershocks are combined to calculate the regional seismic hazard using ground motion prediction equations (GMPEs). Finally, the influence of aftershocks on seismic hazard analysis is examined and considered. The results show that in areas with moderate to strong seismic backgrounds, the influence of aftershocks on probabilistic seismic hazard

20 analysis can exceed 50%. These results suggest that the impact of aftershocks should be properly considered for future probabilistic seismic hazard analyses, especially in areas with moderate to strong seismic activity backgrounds and in areas prone to secondary disasters such as landslides and mudslides.

Keywords: Aftershocks; Omi-R-J model; ETAS model; Monte Carlo method;

25 Seismic hazard analysis.

1 Introduction

Aftershocks are commonly removed from observed earthquake catalog during probabilistic seismic hazard analyses, assuming that earthquakes follow a Poisson distribution. However, the strong aftershocks that follow an earthquake may cause

30 more damage than the mainshock and should not be underestimated. As there is not enough time to repair damages between the mainshock and the subsequent aftershocks,

buildings will suffer cumulative damage from aftershocks, which will lead to additional casualties and property losses (Bi et al., 2022). For example, after the 1976 M7.8 Tangshan earthquake in China, most houses in the aftershock zone collapsed,

35 and the railway lines on the deck of the local bridge were damaged during the M7.1 and M6.9 aftershocks (Lv et al., 2007). The M5.0 aftershock that followed the 2003 M8.0 Hokkaido earthquake in Japan caused a secondary fire disaster due to a spilled tank (Zhao et al., 2005). The M6.3 aftershock that followed the 2010 M7.1 Christchurch earthquake in New Zealand caused damage to buildings, 146 deaths, and

40 over 300 people to go missing (Zhang et al., 2011). Lv et al. (2007) statistically analyzed the aftershocks that followed 21 M >7.0 mainshocks in China and found that the peak ground accelerations caused by aftershocks exceeded the mainshock was 76.2%; that is, aftershocks may cause more severe damage than the mainshock. Therefore, ignoring the impact of aftershocks may underestimate the seismic risk in

45 some areas. The cumulative damage losses caused by strong aftershocks have attracted considerable attention in the field of disaster and catastrophe insurance modelling (Xiong, 2019).

Cornell (1968) proposed the classical probabilistic seismic hazard analysis (PSHA) method, and, based on that work, Wiemer (2000) proposed the aftershocks

50 probabilistic seismic hazard analysis (APSHA). Gallovič & Brokešová (2008) combined the generalized form of the Omori law (Omori, 1894; Utsu, 1961; Utsu et al, 1995) that was given by Shcherbakov et al. (2004), refined the APSHA steps and parameterizations, and analyzed the seismic hazard probability of aftershock that followed several earthquake as case studies. Shen & Yang (2018) used the APSHA

55 method established by Gallovič & Brokešová (2008) to analyze the aftershock seismic hazard probability of the 2017 M7.0 Jiuzhaigou earthquake in China. In addition, many scholars have derived the influence of aftershocks on seismic hazard analysis by using analytical solutions (Yeo & Cornell, 2009; Marzocchi & taroni, 2014; Irvolino et al., 2014; Davoudi et al., 2020; Taroni & Akinci, 2021). Boyd (2012) and Xu & Wu

60 (2017) used the Epistemic-type Aftershock Sequence (ETAS, Ogata, 1988,1998) model to generate catalogs with and without aftershocks. They used a spatially smooth seismicity model to calculate the impact of aftershock clusters for

probabilistic seismic hazard analysis. Canales & Baan (2020) used the Poisson model to generate mainshock sequences and the ETAS model to generate aftershock

65   sequences. By analyzing and comparing the b values of different sequences, the recurrence rate of the largest event can be estimated.

Based on the Seismic Ground Motion Parameter Zoning Map of China (GB18306-2015), this study used the Monte Carlo method to simulate synthetic mainshock sequences. Then, according to the magnitude of the mainshock, the

70   Omi-Reasenberg-Jones (Omi-R-J) aftershock activity model (Omi, 2013, 2016, 2019) is used to simulate the aftershock sequences that follow mainshocks for a certain magnitude threshold. Finally, the mainshocks and the aftershocks are combined to calculate the regional seismic hazard using the ground motion prediction equations (GMPEs). Thus, the influence of aftershocks on seismic hazard analysis is analyzed.

75   Xichang city, one of the three major space launch facilities in China, is located in the Anning River Valley in southwestern Sichuan Province. The Anning River fault and the Zemu River fault run through the city. Historically, there have been three M ≥7.0 earthquakes occured in the region; an M7.0 event in 814, an M7.5 earthquake in 1536 and an M7.5 event in 1850 (Fig. 1). The Anning River fault is one of the main

80   faults in the North-South Sichuan-Yunnan tectonic belt and is also an important fault in Southwest China. According to regional geological data (Li, 1993; He & Ikeda, 2007), the Anning River fault zone is the boundary of different tectonic units from the Paleozoic to Mesozoic eras. The west side of the fault contains the metamorphic complex and magmatic rock belt, and the Mesozoic-Cenozoic sedimentary basin falls

85   on the east side. The Zemu River fault has been active throughout the Holocene (Li, 1997; Du, 2000) and is connected to the Anning River fault zone in the north and the Xiaojiang Fault Zone in the south. The fault has an overall strike of 330 °, a fault plane dip angle of more than 60 ° and a dip direction of northeast or southwest. Since the late Quaternary, the Anning River fault and Zemu River fault have been characterized

90   by continuous strike-slip movements (Xu et al., 2003a; Xu et al., 2003b). The Anning River fault and Zemu River fault are located at the boundary of the central Yunnan secondary block in the Sichuan-Yunnan rhombus block, which controls the focal positions of most nearby earthquakes with M ≥ 7 (Lu et al., 2012).

95 Xichang is located in a strong earthquake prone area. Considering the impact of aftershocks in seismic hazard assessment, it is of critical importance to focus on fortifying areas subject to strong aftershocks, especially against landslides, debris flows and other secondary geological disasters. However, these preparations require the development of accurate disaster prevention technologies.
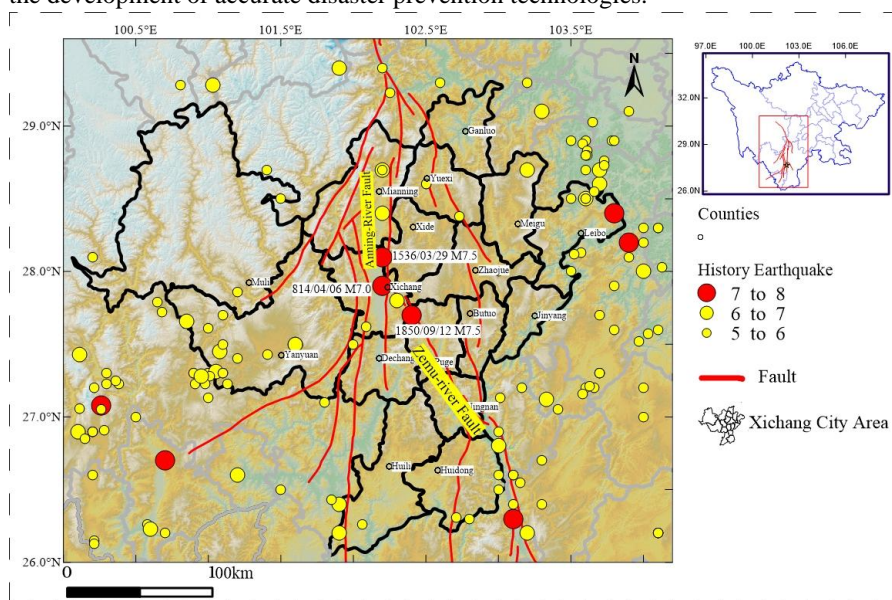
100 **Figure 1 Distribution of seismic events and the tectonic background in Xichang and its surrounding areas**

2. Aftershock activity models and their parameters

2.1 Omi-R-J aftershock sequence model

After moderate or strong earthquakes, when direct information is available, the

105 early activity characteristics of the aftershock sequences are used for sequence type determination (Jiang et al., 2007), strong aftershock prediction (Omi et al., 2013) and short-term aftershock probability prediction (Reasenberg & Jones, 1989; Gerstenberger et al., 2005). These characteristics have important scientific value and practical significance in earthquake relief, regional earthquake risk assessment and

110 understanding of the earthquake sequence itself. Reasenberg and Jones (1989) developed the R-J model to predict the occurrence rate of early aftershocks based on the Omori-Utsu formula (Omori 1894; Utsu 1961) and the Gutenberg-Richard (G-R) law (Gutenberg & Richard, 1944).

According to the R-J model, the aftershock intensity function, with a magnitude
no less than M at time t in the earthquake sequence, can be expressed as:

$$\lambda(t, M) = \frac{k}{(t+c)^p} 10^{-bM} \tag{1}$$

where t is the time after the mainshock. The parameter k controls the activity of
aftershocks, which largely depends on a single aftershock sequence and has little
relationship with the magnitude of the mainshock (Bi et al., 2022). The parameter p
represents the decay degree of the seismic sequence. Parameter c is used to adjust the
incompleteness of the aftershock records within a very short time after the mainshock.
This parameter is a positive and small constant and is negatively correlated with the
focal depth (Shebalin & Narteau, 2017). Parameter b represents the stress
accumulation level (Wiemer & Katsumata, 1999; Enescu et al., 2011). This model is
simple in principle and suitable for estimating the parameters of moderate to strong
earthquake sequences with simple decay laws. As a classical seismic sequence
analysis method, it is widely used in aftershock prediction throughout the world and
for earthquake hazard assessments by the Global Earthquake Model (GEM) project.

After the occurrence of moderate or strong earthquakes, a large number of small
aftershocks will be "submerged" in the early stage, resulting in a reduction in the
completeness of the earthquake catalogs, making it difficult to apply many of the
small earthquakes below the magnitude of completeness. On the basis of the R-J
model, Omi et al. (2013) proposed the "Omi-R-J" model by considering the
aftershocks below the magnitude of completeness during the early stage of the
earthquake sequence in the model parameter fitting and in the aftershock occurrence
rate prediction. Omi et al. (2013) used the expression of the detection rate function
q(M) given by Ogata and Katsura (1993) (OK1993 model) to describe the detection
rate of the incomplete part of the earthquake catalog. The actual recorded earthquake
probability density function can be expressed as:

$$P(M|\beta,\mu,\sigma) = \frac{e^{-\beta M} q(M|\mu,\sigma)}{\int_{-\infty}^{+\infty} e^{-\beta M} q(M|\mu,\sigma)dM} = \frac{e^{-\beta M} q(M|\mu,\sigma)}{e^{(-\beta\mu+\beta^2\sigma^2/2)}/\beta} = \beta e^{-\beta(M-\mu)+\beta^2\sigma^2/2} q(M|\mu,\sigma) \tag{2}$$

where β is equal to $b\ln10$, μ represents the corresponding magnitude when the
detection rate is 50%, σ is the corresponding magnitude dispersion and $\mu+2\sigma$ or $\mu+3\sigma$

is usually used to approximate the minimum magnitude of completeness M_c. In the parameter estimation of formula (2), the "state-space" model developed by Omi et al.

145 (2013) was used to estimate the time varying factor $\mu(t)$. Specifically, $\mu(t)$ is set as the discrete distribution function corresponding to the aftershock time sequence $t_i \leq t \leq t_{i+1}$ $(i=1、2……n)$. The hyperparameter V is set to control the smoothness of the distribution, assuming a priori distribution with a smooth constraint on $\mu(t)$. After the parameters $\beta,\ \sigma,\ and\ V$ are optimized and the maximum a posteriori estimation is

150 performed by the maximum expectation (EM) iterative algorithm, the parameter $\boldsymbol{\mu}=(_{\mu 1,}$ $_{\mu 2……\mu n})^T$ is obtained by Bayesian estimation. Then, the parameter $p,\ c,\ k$ and the standard deviation are further determined by combining the Omori-Utsu formula and the maximum likelihood method.

2.2 ETAS time series model

155 The Epistemic-Type Aftershock Sequence (ETAS) model introduces the idea of self-similarity and assumes that both background earthquakes and triggered earthquakes can stimulate their own aftershocks, and a large number of direct aftershocks and indirect aftershocks (aftershocks of aftershocks) can be generated after a mainshock. Therefore, the ETAS model is constructed with branch point

160 process characteristics (Ogata, 1988; Bi & Jiang, 2019). The conditional intensity function can be expressed as:

$$\lambda(t) = \mu_{ETAS} + K_{ETAS} \sum_{t_i < t} \frac{e^{\alpha_{ETAS}(M_i - M_0)}}{(t - t_i + c_{ETAS})^{p_{ETAS}}}, M_i > M_0 \qquad (3)$$

where $t\text{-}t_i$ represents the elapsed time of seismic event i and K_{ETAS} is a normalized constant that determines the expected number of aftershocks directly

165 triggered by the Mi event. The parameter α_{ETAS} represents the ability of a seismic event to stimulate secondary aftershocks (Ogata 1989; 1992). Compared with isolated earthquakes and main aftershocks, the α_{ETAS} of the swarm-type earthquake sequence is smaller, generally $\alpha_{ETAS} < 1$ (Ogata, 2001), and p_{ETAS} represents the decay degree of the seismic sequence. Parameter c_{ETAS} is used to adjust the incompleteness of

170 aftershock records within a very short time that follows the mainshock. Parameter μ_{ETAS} indicates the occurrence rate of background earthquakes. In the calculation process, when the occurrence rate of background earthquakes in the area is low,

μ_{ETAS}=0 is set to better ensure the stability of parameter fitting.

The maximum likelihood method (MLEs) is used to estimate the parameters

175    $[K_{ETAS}, c_{ETAS}, \alpha_{ETAS}, p_{ETAS}]$ in the ETAS model. The likelihood function L is expressed

as:

$$log L = \sum_{i:S \leq t_i < T} lg\, \lambda(t_i) - \int_S^T \lambda(t)\,dt \qquad (4)$$

2.3 Aftershock sequence models in the Xichang area

Gao (2015) divided the Chinese mainland and its adjacent areas into 29 seismic

180   belts, of which 25 seismic belts are located inside mainland China. Since 1970, the

Xianshuihe East-Yunnan seismic belt, where the Xichang area is located (see Fig. 2),

has experienced six M ≥ 7.0 earthquakes; the 1970 M7.8 Tonghai earthquake in

Yunnan, 1973 M7.6 Luhuo earthquake in Sichuan, 1973 M7.2 Nima earthquake in

Tibet, 1974 M7.1 Daguan earthquake in Yunnan, 1997 M7.4 Nima earthquake in Tibet,

185   and the 2010 M7.1 Yushu earthquake in Qinghai. As the early seismic monitoring

ability in Tibet is limited and the number of recorded aftershocks is low, the two

M7.0+ earthquakes in Tibet cannot be used to fit aftershock parameters. We estimated

the aftershock sequence parameters of the other 4 M7.0+ earthquakes by using the

ETAS model and Omi-R-J model. The results are shown in Table 1 and Table 2. To

190   obtain more samples of aftershock sequence parameters, we use the Omi-R-J model to

calculate the aftershock sequence parameters of 40 M4.5-7.0 earthquakes. The results

are also shown in Table 2.

Table 1 The basic information of four mainshocks with M ≥ 7.0 and aftershock sequence

parameters, as calculated by the ETAS model, from the Xianshuihe East-Yunnan seismic

195   **belt, where the Xichang area is located**

No.	1	2	3	4
Time (BJT)	1970/01/05 01:00:34	1973/02/06 18:37:05	1974/05/11 03:25:16	2010/04/14 07:49:36
Longitude	102.6	100.4	104	96.59
Latitude	24.1	31.5	28.1	33.22
Magnitude	7.8	7.6	7.1	7.3
p	1.27	1.01	0.96	0.99
Error (p)	0.14	0.11	0.07	0.05
c	0.0323	0.0235	0.0053	0.0016
Error (c)	0.0327	0.0214	0.0109	0.0014
k	0.0276	0.0284	0.002	0.036
Error (k)	0.0162	0.0178	0.0022	0.0089
α	1.51	1.22	2.06	0.96

Error (α)	0.24	0.17	0.28	0.11
M_C	3.3	2	2	2
C_0	0.1024	0.0742	0.0491	0.0186
Number of events above M_C	364	585	728	461
Number of events	1278	1044	947	2558

Table 2 The basic information of 44 mainshocks with M ≥ 4.5 and aftershock sequence parameters, as calculated by the Omi-R-J model, from the Xianshuihe East-Yunnan seismic belt, where the Xichang area is located

No.	Time (BJT)	Lon.	Lat.	Mag.	p	Error(p)	c	Error(c)	k	Error(k)	b	Error(b)
1	1970/01/05 01:00:34.34	102.6	24.1	7.8	1.34	0.05	0.3212	0.0553	0.0231	0.012	0.84	0.05
2	1973/02/06 18:37:05.05	100.4	31.5	7.6	0.95	0.04	0.1524	0.0515	0.0004	0.0002	0.92	0.04
3	1974/05/11 03:25:16.16	104	28.1	7.1	0.86	0.02	0.0204	0.0084	0.0085	0.0033	0.78	0.03
4	2010/04/14 07:49:36.36	96.59	33.22	7.3	0.81	0.01	0.0041	0.002	0.0052	0.0014	0.71	0.02
5	1970/07/31 21:10:46.46	103.6	28.53	5.4	0.88	0.09	0.0403	0.0557	0.0103	0.0117	0.99	0.12
6	1971/08/16 12:57:59.59	103.6	28.8	5.9	1.11	0.06	0.9602	0.2154	0.3468	0.1227	0.7	0.04
7	1972/09/30 04:24:39.39	101.57	30.17	5.7	0.69	0.06	0.007	0.016	0.0057	0.0058	0.77	0.09
8	1975/01/12 05:22:27.27	101.53	24.8	5.4	0.67	0.04	0.0223	0.0309	0.0553	0.0212	0.67	0.03
9	1975/01/15 19:34:37.37	101.8	29.43	6.2	0.99	0.07	0.0651	0.0312	0.0128	0.0107	0.81	0.06
10	1975/07/09 21:55:42.42	103.03	23.88	5.3	0.59	0.05	0.0045	0.0099	0.0041	0.0051	0.82	0.06
11	1976/11/07 02:04:05.05	101.08	27.5	6.7	0.69	0.02	0.004	0.0034	0.0195	0.0071	0.83	0.03
12	1976/12/13 14:36:55.55	101.05	27.35	6.4	0.75	0.05	0.0214	0.0263	0.0087	0.0063	0.85	0.06
13	1978/05/20 09:40:52.52	100.3	25.55	5.3	0.62	0.03	0.03	0.0401	0.0385	0.0084	0.84	0.02
14	1978/09/26 05:49:36.36	99.58	29.87	5	0.51	0.06	0.0043	0.0127	0.0203	0.0143	0.88	0.09
15	1980/02/02 20:29:14.14	101.29	27.85	5.8	0.61	0.02	0.0036	0.0018	0.0242	0.0054	0.87	0.02
16	1982/06/16 07:24:32.32	100.03	31.96	6	1.12	0.03	0.0144	0.0037	0.0005	0.0006	1.06	0.07
17	1982/07/03 16:13:31.31	99.87	26.53	5.4	0.8	0.02	0.0138	0.006	0.0328	0.0109	0.83	0.03
18	1983/06/04 17:34:41.41	103.4	26.97	5	0.83	0.07	0.0012	0.0024	0.0185	0.0195	0.68	0.10
19	2001/02/23 08:09:20.20	101.1	29.42	6	0.92	0.1	0.0202	0.043	0.002	0.0052	0.93	0.15
20	2003/06/17 22:46:18.18	102.3	27.87	4.6	0.91	0.1	0.0248	0.0312	0.001	0.0011	1.03	0.10
21	2003/07/21 23:16:00.00	101.2	26	6.2	0.87	0.05	0.0182	0.0179	0.014	0.0088	0.84	0.06
22	2003/10/16 20:28:04.04	101.3	25.92	6.1	0.76	0.06	0.0238	0.0175	0.0076	0.0069	0.9	0.10
23	2003/11/15 02:49:43.43	103.7	27.2	5.1	0.54	0.04	0.0031	0.0076	0.0477	0.0211	0.63	0.04
24	2005/08/05 22:14:43.43	103.1	26.6	5.4	1.15	0.08	0.0999	0.0548	0.0045	0.0047	0.96	0.08
25	2008/08/30 16:30:52.52	101.92	26.28	6.1	1.05	0.08	0.0307	0.0287	0.017	0.0124	0.75	0.06
26	2009/07/09 19:19:14.14	101.03	25.6	6.3	1.14	0.06	0.1662	0.0633	0.0137	0.0063	0.78	0.03
27	2010/02/25 12:56:51.51	101.94	25.42	5.2	0.99	0.05	0.0019	0.0015	0.0051	0.003	0.79	0.07
28	2012/06/24 15:59:34.34	100.69	27.71	5.7	1.14	0.09	0.244	0.0489	0.0299	0.0206	0.96	0.02
29	2012/09/07 11:19:41.41	103.97	27.51	5.7	0.7	0.02	0.0043	0.0027	0.0606	0.0097	0.7	0.02
30	2013/01/18 20:42:50.50	99.4	30.95	5.5	1.2	0.08	0.0091	0.0059	0.0043	0.0058	0.86	0.10
31	2013/08/31 08:04:17.17	99.35	28.15	5.9	0.81	0.01	0.0028	0.0015	0.0156	0.0022	0.98	0.01
32	2014/01/15 03:17:46.46	101.17	26.86	4.5	0.99	0.09	0.0032	0.0136	0.0048	0.0082	0.74	0.11
33	2014/05/07	101.92	25.49	4.7	0.88	0.09	0.015	0.0194	0.0053	0.0069	0.86	0.13

	22:11:42.42											
34	2014/08/03 16:30:12.12	103.33	27.11	6.6	0.73	0.02	0.0047	0.0029	0.0264	0.0075	0.72	0.02
35	2014/08/17 06:07:59.59	103.51	28.12	5.2	0.84	0.07	0.011	0.0298	0.0258	0.0137	0.75	0.05
36	2014/10/01 09:23:29.29	102.74	28.38	5.2	1.14	0.1	0.1486	0.0976	0.0104	0.0083	0.78	0.07
37	2014/11/22 16:55:28.28	101.68	30.29	6.4	0.53	0.01	0.0043	0.0054	0.0004	0.0001	1.03	0.02
38	2016/09/23 00:47:13.13	99.6	30.08	5.2	1.01	0.03	0.0192	0.0073	0.0214	0.0095	0.92	0.05
39	2017/02/08 19:11:39.39	103.37	27.09	4.9	0.84	0.1	0.0359	0.058	0.0035	0.0042	0.96	0.13
40	2018/05/16 16:46:12.12	102.31	29.23	4.5	1.16	0.05	0.0023	0.0011	0.0138	0.0072	0.82	0.07
41	2018/08/13 01:44:25.25	102.72	24.18	5.1	1.14	0.05	0.1091	0.0315	0.1725	0.0418	0.61	0.02
42	2018/10/17 13:29:19.19	102.25	25.89	4.6	0.85	0.12	0.0305	0.143	0.0035	0.005	0.94	0.11
43	2018/10/31 16:29:56.56	102.09	27.62	5.1	1.4	0.1	1.2964	0.3135	0.0006	0.0008	1.06	0.06
44	2018/12/13 23:32:52.52	98.84	29.6	4.9	1.08	0.07	0.009	0.0061	0.0192	0.0179	0.83	0.11

3 Probabilistic seismic hazard analysis method considering aftershocks

Wu et al. (2020) used the Monte Carlo method to simulate synthetic earthquake catalogs for probabilistic seismic hazard analysis based on the Seismic Ground Motion Parameters Zonation Map of China (GB18306-2015). See reference Wu et al. (2020) for the specific seismicity model and Monte Carlo procedure. On this basis, this paper further considers aftershocks in seismic hazard analysis.

The seismic source zone model used by the Seismic Ground Motion Parameters Zonation Map of China (GB18306-2015) is based on seismological and geological data for China. To reflect the heterogeneity of potential seismicity and describe the structural complexity more faithfully, the model adopts a three-level delineation of seismic belts, uses background and structural sources, and considers the tectonic differences between eastern and western China (Zhou et al. 2013). The spatial relationship of the three source levels is as follows (see Fig. 2): the base layer is the seismic belt (seismic statistical area), which is used to reflect the overall statistical characteristics of seismicity; the middle layer is the background potential sources, which are used to reflect the differences in seismic characteristics of small- and moderate-magnitude earthquakes under different tectonic conditions; and the upper layer consists of the structural potential sources, which are used to reflect the small scale spatial seismic heterogeneity caused by the differences in local seismic structural conditions. This is a peculiar property of the seismicity model used for probabilistic seismic hazard assessment in China (CPSHA). Figure 2 shows the spatial

distribution of the potential sources for the Xianshuihe East-Yunnan seismic belt
where the Xichang area is located.
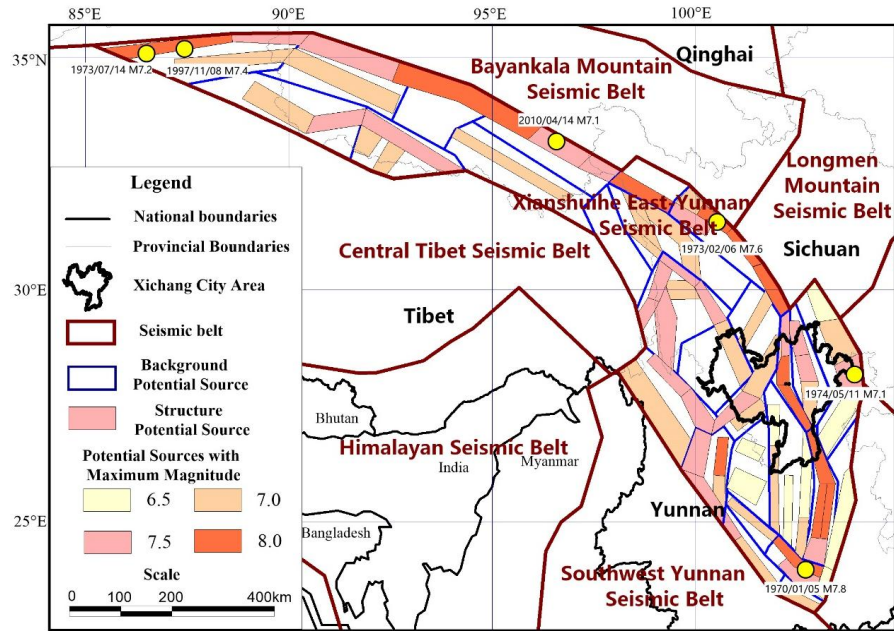
**Figure 2 The spatial distribution of the potential sources for the Xianshuihe East-Yunnan
seismic belt where the Xichang area is located, and six M ≥ 7.0 earthquakes in the belt since
1970**

Since there are only a few strong earthquakes with M ≥ 7 in the Xianshuihe
East-Yunnan seismic belt, the Omi-R-J model is selected as the aftershock parameter
model. According to the spatial division of the Seismic Ground Motion Parameters
Zonation Map of China (GB18306-2015), the median values of the p, c, K and b
values (see Table 2) used in the Omi-R-J model (Omi et al., 2013, 2016, 2019) for the
aftershock sequence samples from the Xianshuihe East-Yunnan seismic belt are
0.8747, 0.0187, 0.0133 and 0.8361, respectively. The aftershock sequences are
generated according to these median values and the following steps:

(1) The mainshock sequences are simulated by the Monte Carlo method based on the
Seismic Ground Motion Parameters Zonation Map of China (GB18306-2015).
Each synthetic sequence represents a 1-year possible distribution of earthquakes in
the region that is consistent with the seismicity model (Wu et al., 2020).
Considering the destructiveness of the earthquake, when the magnitude threshold

240   for the mainshock is met (M ≥ 6.0 in this study), the aftershock sequence sampling
       is started.

(2) The minimum magnitude of the aftershock sequence is set to 4.0, and the
    maximum magnitude is equal to the magnitude of the mainshock. The aftershock
    sequence satisfies the magnitude-frequency relationship $N(M)=10^{a-bM}$. The

245   aftershock occurrence time t is within 30 days after the mainshock and follows the
    Omori-Utsu formula $N(t)=\dfrac{K}{(t+c)^{p}}$. According to the median value of p, c, K and
    b and the upper limit of magnitude of the potential sources, the magnitude and
    time series of aftershocks with M ≥ 4 are simulated.

(3) According to the empirical relationship between the magnitude of the mainshock

250   and the rupture scale (Wells & Coppersmith, 1994), the rupture length and width
    are calculated. The rupture strike is taken as the direction of the potential source
    area where the mainshock is located, and the model of Felzer & Brodsky (2006) is
    adopted; that is, the aftershock density decays exponentially with increasing
    distance r from the fault, $\rho(r) = cr^{-n}$, where n is 1.37, and c is a constant. Thus,

255   the locations of the aftershock epicenters can be determined.

       Figure 3 (a) shows a schematic diagram of the spatial distribution of 1-year
   mainshocks with M ≥ 6 sampled 100 times. The yellow star in the figure is the
   location of the mainshock. Figure 3 (b) is a schematic diagram of the spatial
   distribution of the corresponding aftershocks. The small blue dot in the figure is the

260   aftershock corresponding to the mainshock. The distribution direction of the
   aftershocks refers to the strike of the potential source area where the mainshock is
   located. In this study, considering the destructiveness of the earthquake, when the
   magnitude of the mainshock is ≥ 6.0, random sampling of the aftershock sequence is
   begun, and the sampling time is set within 30 days after the mainshock. The model

265   program user interface can be used to adjust and refine the aftershock model in order
   to account for random aftershock sequences in the future that may have different
   requirements. To ensure the stability of the results, we conducted 5 million 1-year
   samplings.

270   (a)

(b)
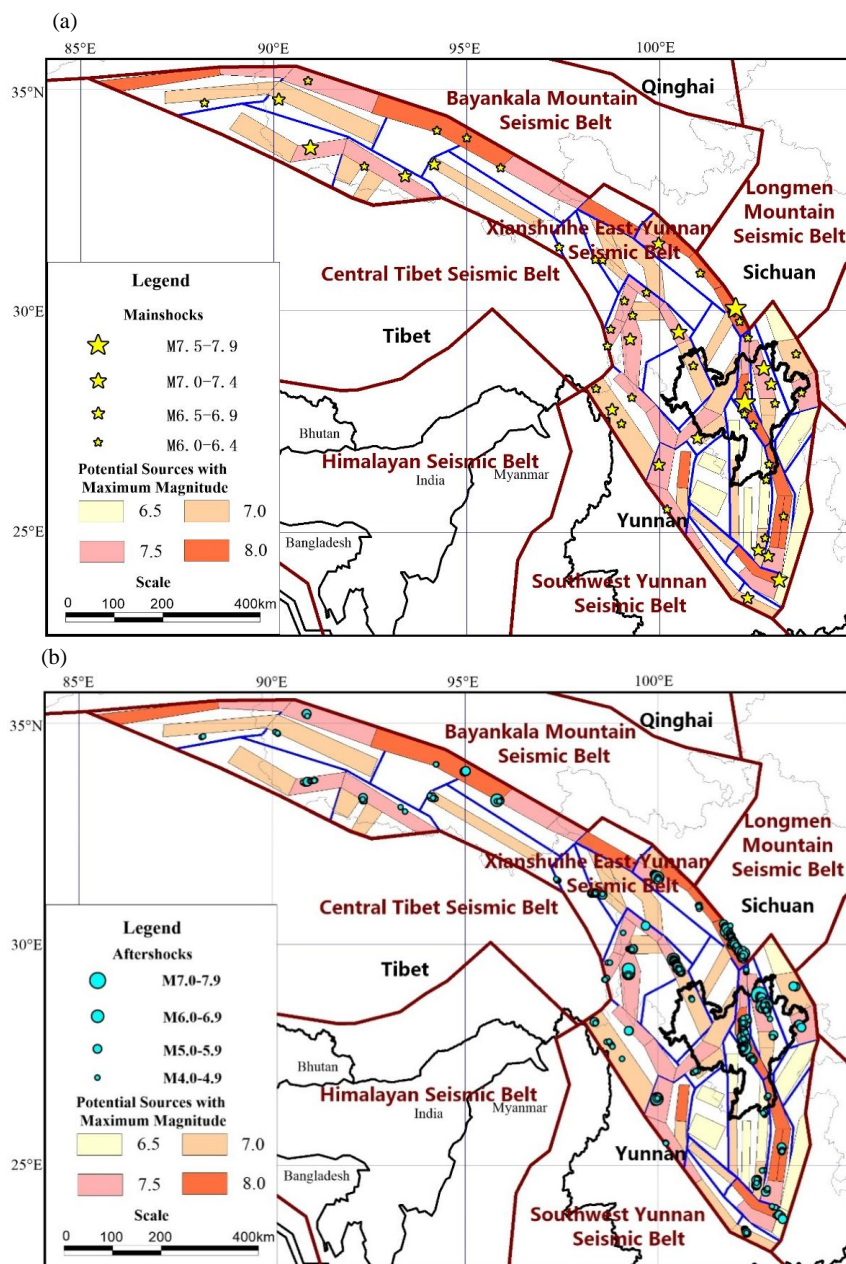
Figure 3 Distribution of 1-year mainshocks with M ≥ 6 and their corresponding aftershocks in 100 samplings

After the aftershocks are obtained, the main aftershocks are combined, the ground motion value of the site is calculated by using the ground motion prediction

equations (GMPEs), and the exceedance probability for a specific case is counted;

280   thus, a probabilistic seismic hazard analysis that considers aftershocks can be carried

out. Figure 4 shows the calculation process for this analysis. According to the Seismic

Ground Motion Parameters Zonation Map of China (GB18306-2015), the GMPEs of

peak ground acceleration (PGA) suitable for the Xichang area are as follows (Xiao,

2011):

285   When $M < 6.5$,

$$\begin{cases} \log_{10} \bar{G}_l(M,R) = 2.331 + 0.646M - 2.431\log\left(R + 2.647\exp(0.366M)\right) \\ \log_{10} \bar{G}_s(M,R) = 1.017 + 0.614M - 1.866\log\left(R + 0.612\exp(0.457M)\right) \end{cases}, \quad (5\text{-}1)$$

When $M \geq 6.5$,

$$\begin{cases} \log_{10} \bar{G}_l(M,R) = 3.846 + 0.413M - 2.431\log\left(R + 2.647\exp(0.366M)\right) \\ \log_{10} \bar{G}_s(M,R) = 2.499 + 0.388M - 1.866\log\left(R + 0.612\exp(0.457M)\right) \end{cases}, \quad (5\text{-}2)$$

where $G(M,R)$ is the peak ground acceleration (PGA), M is the magnitude, R

290   is the epicentral distance, and the other coefficients are obtained by regression.
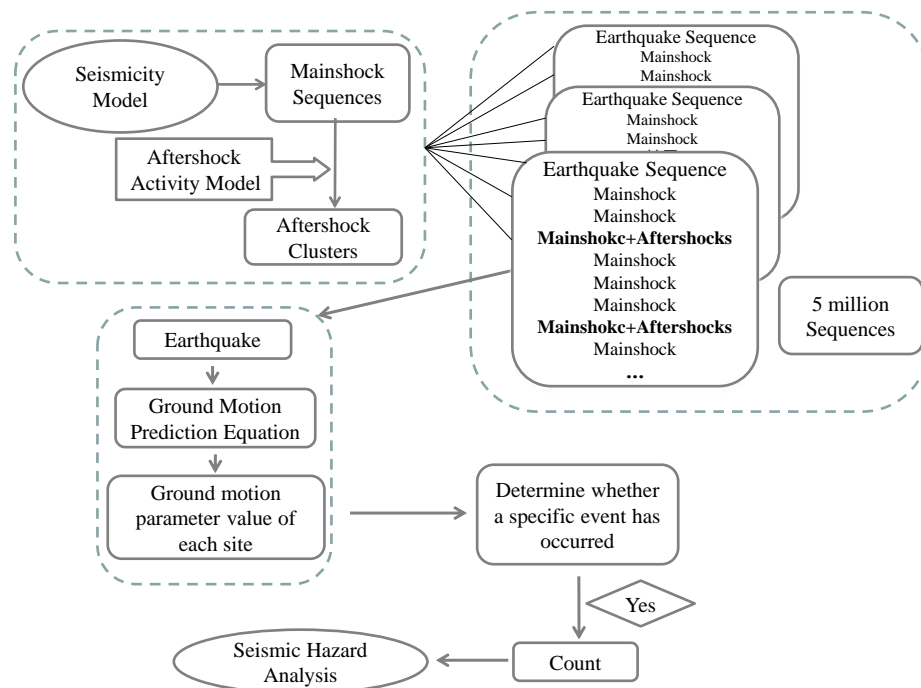
Figure 4 Flow chart of seismic hazard analysis when considering aftershocks

4 Influence of aftershocks on probabilistic seismic hazard analysis

295   To calculate the impact of aftershocks on seismic hazard analysis, Xichang and its surrounding areas were divided into $0.1°\times0.1°$ grid, and the PGA values of the 50-year exceedance probability of 10% and 2% were calculated for each grid point. The results of the calculation with and without aftershocks were compared.

        Figure 5 shows the PGA contour map of the 50-year exceedance probability of

300   10% in Xichang and its surrounding areas calculated without and with aftershocks as well as the aftershock impact rate distribution map.

        To calculate the aftershock impact rate, we take the difference between the calculation results of the aftershock model and the calculation results of model without aftershocks and divide that value by the calculation results of model without

305   aftershocks.

        The maximum impact rate of aftershocks in Xichang and its surrounding areas is 0.55, the minimum is 0, and the average is 0.10. Aftershocks have the largest impact in the Xichang urban area, where there was an M7 earthquake in 814, an M7.5 earthquake in 1536 and an M7.5 earthquake in 1850. The upper limit of magnitude of

310   the potential source area is 8.0.

        Figure 6 shows the PGA contour map of the 50-year exceedance probability of 2% in Xichang and its surrounding areas calculated with and without aftershocks. Additionally, this figure also shows the aftershock impact rate distribution map. The maximum impact rate of aftershocks in Xichang and its surrounding areas is 0.72, the

315   minimum is 0, and the average is 0.10. The greatest impact of aftershocks is also in the Xichang urban area, where there was an M7 earthquake in 814, an M7.5 earthquake in 1536 and an M7.5 earthquake in 1850. The upper limit of magnitude of the potential source area is 8.0. In this calculation, only mainshocks with M≥6.0 can generate aftershocks. Therefore, the calculated results are consistent with the

320   aftershock model. The seismic hazards for sites with different seismic backgrounds are affected by aftershocks to different degrees.

(a) without aftershocks
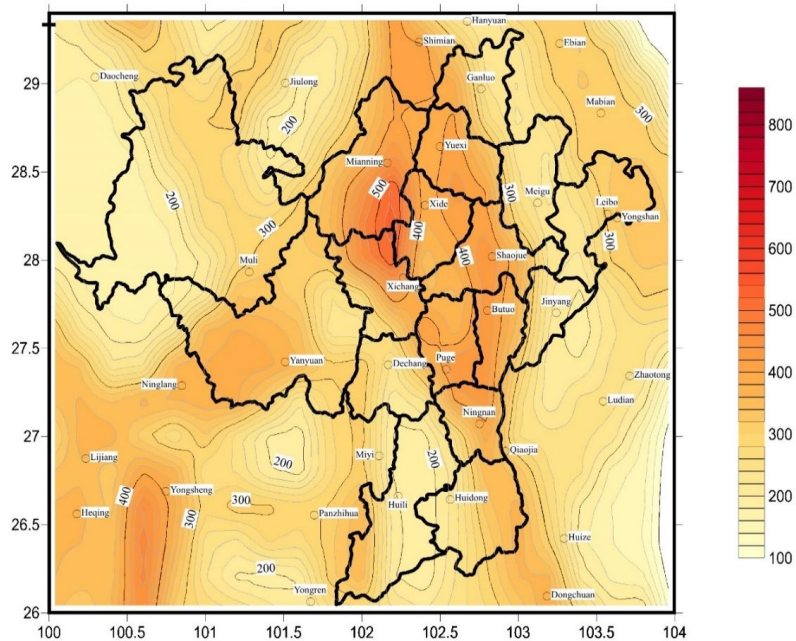
325

(b) with aftershocks
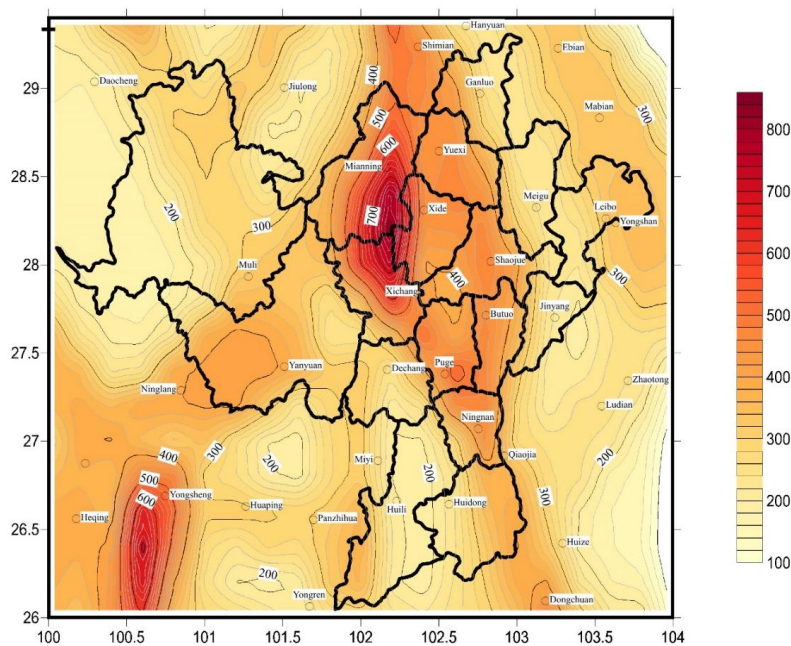
330   (c) the aftershock impact rate
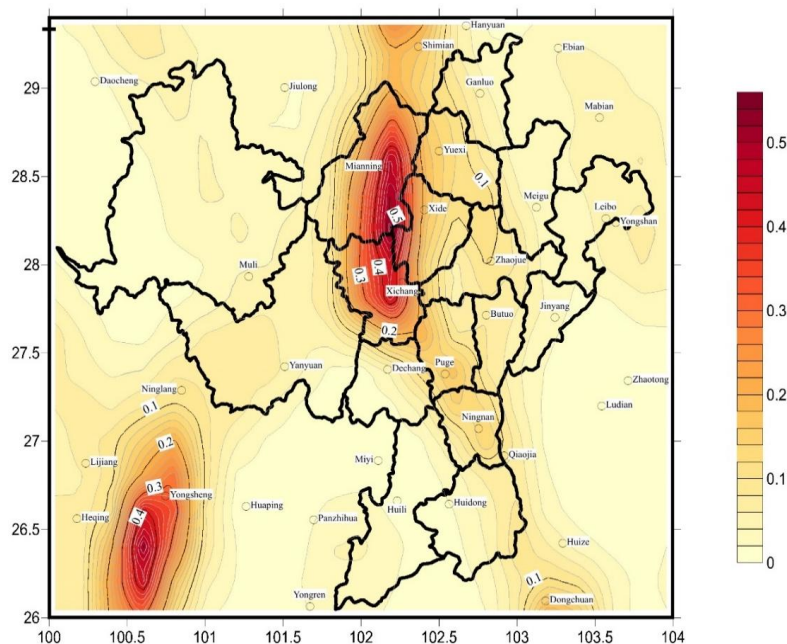
Figure 5 Comparison of the aftershock impacts on PGA (gal) with a 10% exceedance

probability over 50 years in Xichang and its surrounding areas

(a) without aftershocks
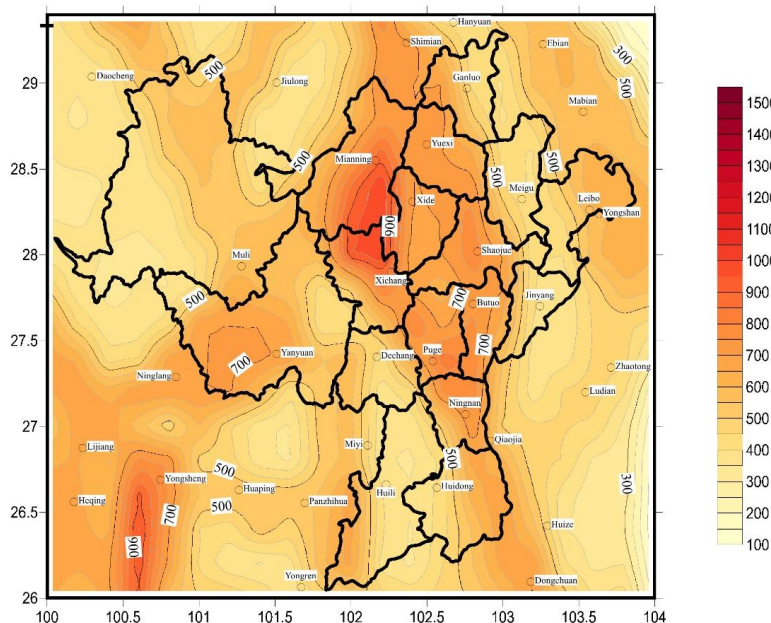
335

(b) with aftershocks
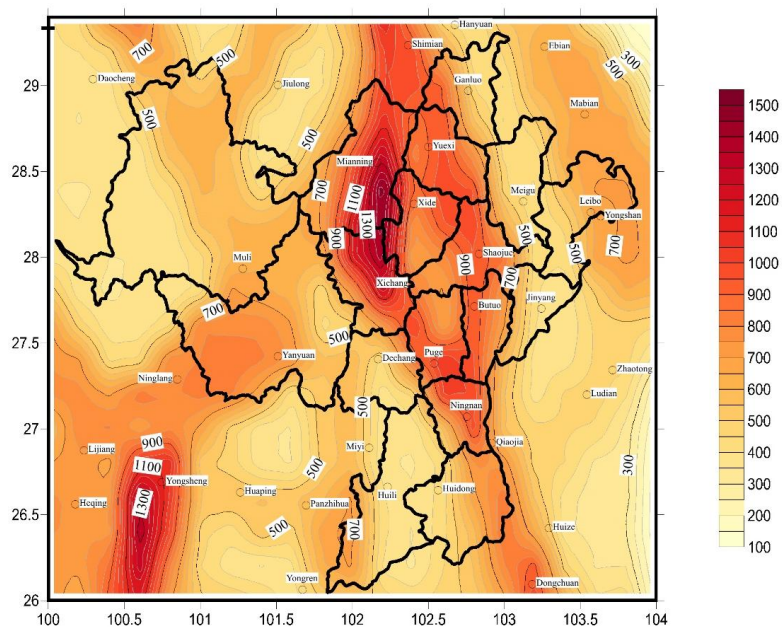
(c) the aftershock impact rate
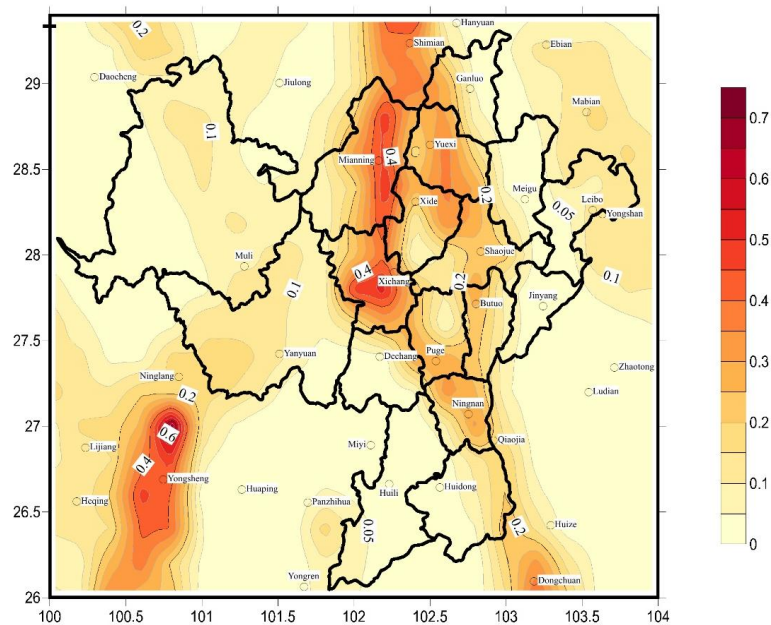
340 **Figure 6 Comparison of the aftershock impacts on PGA (gal) with a 2% exceedance**

probability over 50 years in Xichang and its surrounding areas

5 Discussion & conclusions

In this study, a probabilistic seismic hazard analysis based on the Monte Carlo method was combined with the Omi-R-J model to systematically study how aftershocks impact seismic hazard analyses in Xichang city and the surrounding areas. The results show that in areas with moderate to strong seismic backgrounds, the influence of aftershocks on probabilistic seismic hazard analysis can exceed 50%. Aftershocks are typically ignored for traditional probabilistic seismic hazard analyses, which underestimates the seismic hazard to some extent and may cause potential risks. Our results suggest that the impact of aftershocks should be properly considered during future probabilistic seismic hazard analyses, especially in areas with moderate to strong seismic activity backgrounds and in areas prone to secondary disasters such as landslides and mudslides.

The model settings adopted for the calculation processes presented in this study can be modified according to the actual situation and specific requirements. The Monte Carlo method is highly adaptable and can take into account different parameters for different models. In future work, we can attempt to adjust the initial magnitude of the mainshock and the aftershock. Additionally, we can adjust the duration of the aftershock and use different mainshock models and aftershock models to study how aftershocks impact probabilistic seismic hazard analysis.

This work provides a scientific basis for governmental departments to minimize disaster losses and formulate corresponding earthquake prevention and disaster mitigation measures. Furthermore, this work plays a very important role in engineering decision making and judgment, the implementation of catastrophe insurance, etc.

Data availability

All raw data can be provided by the corresponding authors upon request.

Author contributions

All authors contributed to the study conception and design. Material preparation, data collection and analysis were performed by Qing Wu and Guijuan Lai. The first draft of the manuscript was written by Qing Wu and all authors commented on previous versions of the manuscript. All authors read and approved the final

manuscript.

Competing interests

375 The authors declare that they have no conflict of interest.

Acknowledgments

We thank the Compiling Committee of the Seismic Ground Motion Parameters Zonation Map of China for providing the seismic source zone model, seismicity model and GMPE model data. Thank you to Dr. Zongchao Li for his help in drawing

380 the map showing the seismic event distribution and tectonic background in Xichang and its surrounding areas.

Financial support

This work was supported by the Key R&D Program of Xinjiang Uygur Autonomous Region (grant number 2020B03006-4), the Science and Technology Basic Resources

385 Investigation Program of China (grant number 2018FY100504), and the Special Fund of the Institute of Geophysics, China Earthquake Administration (grant number DQJB22Z02-8, DQJB22Z03-4).

References

Bi, J. M., & Jiang, C. S.: Distribution characteristics of earthquake sequence

390 parameters in North China. *Chinese Journal of Geophysics*, 62(11), 4300-4312, 2019. (in Chinese)

Bi, J. M., Jiang, C. S., Lai, G. J., et al.: Effectiveness evaluation and constrains of early aftershock probability forecasting for strong earthquakes in continental China. *Chinese Journal of Geophysics*, 65(7), 2532-2545,2022. (in Chinese)

395 Boyd, O. S.: Including foreshocks and aftershocks in time-independent probabilistic seismic-hazard analyses. *Bulletin of the Seismological Society of America*, 102(3), 909-917, 2012.

Canales, M. R., & Baan, M. V. D.: Are aftershock sequences pertinent to long-term seismic hazard assessments? Insights from the temporal ETAS model. *Journal of

400 Geophysical Research: Solid Earth*, 125, e2019JB019095, 2020.

Cornell, C. A.: Engineering seismic risk analysis. *Bulletin of the Seismological Society of America*, 58(5), 1583–1606, 1968.

Davoudi, N., Tavakoli, H. R., Zare, M., Jalilian, A.: Aftershock probabilistic seismic

hazard analysis for Bushehr province in Iran using ETAS model. *Natural Hazards*, 100, 1159-1170, 2020.

Du, P. S.: Recurrence interval on macroearthquake along the active fault of Zemuhe. *Earthquake Research in Sichuan*, 1-2, 102-118, 2000. (in Chinese)

Enescu, B., Enescu, D., Ito, K.: Values of b and p: their variations and relation to physical processes for earthquakes in Japan and Romania. *Romanian Journal of Physics*, 56(34): 590-608, 2011.

Felzer, K., & Brodsky, E.: Decay of aftershock density with distance indicates triggering by dynamic stress. *Nature*, 441(7094), 735-8, 2006.

Gallovič, F., & Brokešová, J.: Probabilistic aftershock hazard assessment Ⅰ: Numerical testing of methodological features. *J Seismol*, 12(1), 53–64, 2008.

Gao, M. T. (editor in chief).: Publicity and implementation textbook of the Seismic Ground Motion Parameters Zonation Map of China (GB18306-2015), V1.0, Standards Press of China, ISBN: 978-7-5066-7888-9, 2015. (in Chinese)

Gerstenberger, M. C., Wiemer, S., Jones, L. M., et al.: Real-time forecasts of tomorrow's earthquakes in California. *Nature*, 435, 328–331. DOI:10.1038/nature03622, 2005.

Gutenberg, B., & Richter, C. F.: Frequency of earthquakes in California. *Bulletin of the Seismological Society of America*, 34(4), 185–188. doi: 10.1038/156371a0, 1944.

He, H. L., & Ikeda, Y.: Faulting on the Anninghe fault zone, southwest China in late quaternary and its movement model. *Acta Seismologica Sinica*, 29(5), 537-548, 2007. (in Chinese)

Iervolino, I., Giorgio, M., Polidoro, B.: Sequence-based probabilistic seismic hazard analysis, short note. *Bulletin of the Seismological Society of America*, 104(2), 1006-1012, 2014.

Jiang, H. K., Zheng, J. C., Wu, Q., et al.: Earlier statistical features of ETAS model parameters and their seismological meanings. *Chinese Journal of Geophysics*, 50(6), 1778-1786, 2007. (in Chinese)

Li, P., & Wang, L. M.: Discussion on the basic characteristics of seismogeology in Western Sichuan-Yunnan. Beijing: Seismological Press, 1977. (in Chinese)

435   Li, P.: Xianshuihe-Xiaojiang fault zone. Beijing: Seismological Press, 1993. (in Chinese)

Lu, P., Yuan, Y. F., Yuan, H. K., et al.: Probabilistic estimate of strong earthquake risk in the Anninghe-Zemuhe tectonic zone. *Earthquake*, 32(4), 62-72, 2012. (in Chinese)

440   Lv, X. J., Gao, M. T., Gao, Z. W., Mi, S. T.: Comparison of the spatial distribution of ground motion between mainshocks and strong aftershocks. *Acta Seismologica Sinica*, 29(3), 295-301, 2007. (in Chinese)

Marzocchi, W., & Taroni, M.: Some thoughts on declustering in probabilistic seismic hazard analysis. *Bulletin of the Seismological Society of America*, 104(4),
445   1838-1845, 2014.

Ogata, Y.: Statistical models for earthquake occurrences and residual analysis for point processes. *Journal of the American Statistical Association*, 83(401), 9–27, 1988.

Ogata, Y.: Statistical model for standard seismicity and detection of anomalies by
450   residual analysis. *Tectonophysics*, 169(1-3), 159-174, 1989.

Ogata, Y.: Detection of precursory relative quiescence before great earthquakes through a statistical model. *Journal of Geophysical Research: Solid Earth*, 97(B13) , 19845-19871, 1992.

Ogata, Y., & Katsura, K.: Analysis of temporal and spatial heterogeneity of magnitude
455   frequency distribution inferred from earthquake catalogues. *Geophysical Journal International*, 113(3), 727-738, 1993.

Ogata, Y.: Space-time point-process models for earthquake occurrences. *Annals of the Institute of Statistical Mathematics*, 50(2), 379–402, 1998.

Ogata, Y.: Increased probability of large earthquakes near aftershock regions with
460   relative quiescence. *Journal of Geophysical Research*, 106, 8729-8744, 2001.

Omi, T., Ogata, Y., Hirata, Y., et al.: Forecasting large aftershocks within one day after the mainshock. *Scientific Reports*, 3, 2218, doi: 10.1038/srep02218, 2013.

Omi, T., Ogata, Y., Shiomi, K., et al.: Automatic aftershock forecasting: A test using real-time seismicity data in Japan. *Bulletin of the Seismological Society of*
465   *America*, 106(6), 2450-2458, doi: 10.1785/0120160100, 2016.

Omi, T., Ogata, Y., Shiomi, K.: Implementation of a real-time system for automatic aftershock forecasting in Japan. *Seismological Research Letters*, 90(1), 242-250, 2019.

Omori, F.: On after-shocks of earthquakes. *J Coll Sci Imp Univ Tokyo*, 7, 111–200, 1894.

Reasenberg, P. A., & Jones, L. M.: Earthquake hazard after a mainshock in California. *Science*, 243, 1173-1176, 1989.

Shebalin, P., & Narteau, C.: Depth dependent stress revealed by aftershocks. *Nature Communications*, 8(1), 1317, 2017.

Shen, W. H., & Yang, F.: Probabilistic aftershock hazard assessment for Jiuzhaigou MS7.0 earthquake in 2017. *Acta Seismologica Sinica*, 40(5), 654−663. doi:10.11939/jass.20170204, 2018.

Shcherbakov, R., Turcotte, D. L., Rundle, J. B.: Ageneralized Omori 's law for earthquake after shockdecay. *Geophys Res Lett*, 31(11), L11613, 2004.

Taroni, M., & Akinci, A.: Good practices in PSHA: declustering, b-value estimation, foreshocks and aftershocks inclusion; a case study in Italy. *Geophys. J. Int.*, 224, 1174-1187, 2021.

Utsu, T.: A statistical study on the occurrence of aftershocks. *Geophys Mag*, 30, 521–605, 1961.

Utsu, T., & Ogata, Y., Matsu'ura, R. S.: The centenary of the Omori formula for a decay law of aftershock activity. *J Phys Earth*, 43(1), 1–33, 1995.

Well, D. L., & Coppersmith, K. J.: New empirical relationships among magnitude, rupture length, rupture width, rupture area, and surface displacement. *Bulletin of the Seismological Society of America*, 84(4), 974-1002, 1994.

Wiemer, S.: Introducing probabilistic aftershock hazard mapping. *Geophys Res Lett,* 27(20), 3405–3408, 2000.

Wiemer, S., & Katsumata, K.: Spatial variability of seismicity parameters in aftershock zones. *Journal of Geophysical Research: Solid Earth,* 104(B6), 13135-13151, 1999.

Wu, Q., Wu, J., Gao, M. T.: Correlation analysis of earthquake impacts on a nuclear power plant cluster in Fujian province, China. *Environmental Research*, 187, doi:

10.1016/j.envres.2020.109689, 2020.

Xiao, L.: Study on the attenuation relationship of horizontal ground motion parameters near the source of rock site. Doctor's Degree Thesis. Beijing: Institute

500   of Geophysics, China Earthquake Administration, 120, 2011. (in Chinese)

Xiong, Z. H.: The study and application of catastrophe model for earthquake insurance. Doctor's Degree Thesis. Beijing: Institute of Geophysics, China Earthquake Administration, 2019. (in Chinese)

Xu, W. J., & Wu, J.: Effect of temporal-spatial clustering of aftershocks on the

505   analysis of probabilistic seismic hazard. *Chinese Journal of Geophysics*, 60(8), 3110-3118, 2017. (in Chinese)

Xu, X. W., Wen, X. Z., Zheng, R. Z., et al.: The latest tectonic variation pattern and its dynamic source of active blocks in Sichuan-Yunnan region. *Science China (Series D)*, (33 Z), 151-162, 2003. (in Chinese), a

510 Xu, X. W., Cheng, G. L., Yu, G. H., et al.: Tectonic and paleomagnetic evidence for the clockwise rotation of the Sichuan-Yunnan rhombic block. *Seismology and Geology*, 25(1), 61-70, 2003. (in Chinese), b

Yeo, G. L., & Cornell, C. A.: A probabilistic framework for quantification of aftershock ground-motion hazard in California: methodology and parametric

515   study. *Earthquake Engng Struct Dyn*, 38, 45–60, 2009.

Zhao, J. B.: Damage assessment of reinforced concrete frame structures under main and aftershocks. Master's Degree Thesis. Beijing: Institute of Geophysics, China Earthquake Administration, 2005.

Zhang, C. J., Hou, Y. Y., Hu, B., Xu, H. H., Wang, D. B.: Analysis on the seismic

520   activities and hazards of M7.1 earthquake, 2010 and M6.3 earthquake, 2011 in New Zealand. *Recent Developments in World Seismology*, 4, 44-51, 2011. (in Chinese)

Zhou, B. G., Chen, G. X., Gao, Z. W., et al.: The technical highlights in identifying the potential seismic sources for the update of national seismic zoning map of

525   China. *Technol Earthq Disaster Prev*, 8(2), 113–124, 2013. (in Chinese)